MODELLING AND PRESTACK REVERSE-TIME MIGRATION BY THE RAPID EXPANSION METHOD WITH TIME-STEPPING

E. Tessmer

email: *ekkehart.tessmer@zmaw.de*

keywords: *seismic modelling, reverse-time migration, wave equation, Poynting vector, time-stepping*

ABSTRACT

Reverse-time migration is based on seismic forward modelling algorithms, where spatial derivatives are usually calculated by finite-differences or by the Fourier method. Time integration is in general done by finite-difference time-stepping of low orders. If the spatial derivatives are calculated by high-order methods and time-stepping is based on low-order methods there is an imbalance which may require that the time-step size needs to be chosen very small to avoid numerical dispersion. As a result computing times increase. Using the Rapid Expansion Method avoids numerical dispersion if the number of expansion terms is chosen properly. We show by comparisons with analytical solutions that the Rapid Expansion Method is preferable especially at larger propagation times. For reverse-time migration it may be desirable to use the Poynting vector information for estimation of opening angles to improve the image quality. In the solution of the wave equation this requires to calculate not only the pressure wave field but in addition its time derivative. We show that the Rapid Expansion Method can be easily extended to also provide this time derivative at negligible extra cost.

INTRODUCTION

The accuracy and efficiency of reverse-time migration strongly depends on the algorithm used for numerical seismic forward modelling. Both, the way in which spatial derivatives are computed as well as the kind of temporal time-integration affect the quality of the numerical results.

Seismic modelling methods which are based on regular grids often use low order finite-difference (FD) time integration techniques. This applies for modelling algorithms where the spatial derivatives are calculated using finite-differences or by pseudo-spectral approaches like the Fourier method. If the approximations of spatial derivatives are calculated by higher order FD techniques or by the Fourier method there is an imbalance of the accuracies between the temporal and the spatial approximations. This can lead to unwanted numerical dispersion and hence inaccurate results for large propagation times (Dablain (1986), Crase (1990)). Kosloff et al. (1989) introduced the Rapid Expansion Method (REM) for solving the acoustic wave equation or the elastodynamic equations of motion with a source term and with zero initial conditions. This method has very high accuracy with respect to the temporal extrapolation. In fact the combination of the REM approach and the Fourier method allows to obtain modelling results which are free of numerical dispersion. The REM time integration basically starts from the formal solution of the governing partial differential equations and expands the solution into Chebyshev polynomials. This is much more efficient than using Taylor expansions.

Since reverse-time migration (RTM) is based on seismic modelling algorithms it is desirable to also use a highly accurate numerical modelling approach for this purpose. Recently, Pestana and Stoffa (2009) described how to implement the REM approach in a time-stepping manner. For RTM this implementation is necessary since for the reverse modelling many sources with many different time-histories need to be applied at the receiver locations. This is incompatible with the original REM implementation of Kosloff et al. (1989) since in this approach the source must be separable in space and time. Therefore, Pestana and

Stoffa (2009) start from the formal solution of homogeneous differential equations. In this approach the samples of the time-reversed seismograms are used to modify the initial conditions time-step for time-step at the respective receiver locations.
Pestana and Stoffa (2009) discuss the choice of the number of expansion terms by means of migrated images. To be on more solid ground to make a proper choice of the number of expansion terms in the present paper modelling results are compared to analytic solutions for simple geometries. Moreover, the computations of Chebyshev polynomials appears unnecessarily complicated in Pestana and Stoffa (2009). Moreover, the computation of Bessel functions is not appropriate since small arguments are assumed which is not always the case. A simple and accurate method to evaluate Bessel functions adopted from Abramowitz and Stegun (1972) is given in the Appendix A.
In the first chapter a short review of the theory of time-stepping with the REM approach is given. In the second chapter 2D modelling examples are compared to analytic solutions for FD time-stepping as well as for the REM approach. Furthermore, it is examined how to chose the number of expansion terms to aim at modelling results which are free of numerical dispersion and truncation errors.
In the third chapter it is shown that REM also allows to calculate first time derivatives of the solution of the wave equation. This is useful, e.g., in RTM when Poynting vectors need to be computed.
The fourth chapter demonstrates the application of prestack RTM using the REM approach to a simple synthetic 2D example. Imaging results obtained by incorporation of Poynting vectors (Yoon et al., 2004) into the imaging condition are compared to images based on the full range of scattering angles.
The last chapter summarizes the conclusions.

SOLVING THE WAVE EQUATION BY THE RAPID EXPANSION METHOD WITH TIME-STEPPING

The Rapid Expansion Method, first presented in Kosloff et al. (1989), solves the acoustic wave equation or the equations of dynamic elasticity with zero initial conditions. If these equations are written in an operator notation they read:

$$\frac{\partial^2 \mathbf{u}}{\partial t^2} = -\mathbf{L^2 u} + \mathbf{f}. \tag{1}$$

$\mathbf{u}$ and $\mathbf{f}$ denote the displacements and the source term, respectively. In case of, e.g., the 2D constant-density acoustic wave equation the operator $-\mathbf{L^2}$ is given by:

$$-\mathbf{L^2} = v^2 \left(\frac{\partial^2}{\partial x^2} + \frac{\partial^2}{\partial z^2} \right). \tag{2}$$

The quantity $\mathbf{u}$ in equation 1 is then replaced by the pressure $\mathbf{p}$. v is the acoustic velocity. In case of variable-density acoustic modelling or elastic modelling the operator $-\mathbf{L^2}$ has a different form (see Kosloff et al. (1989)).
$\mathbf{u}$ and $\mathbf{f}$ are vectors of size $n_x \times n_z$, where n_x and n_z are the number of grid points in the respective directions. The operator $-\mathbf{L^2}$ is a $n \times n$ matrix, where $n = n_x \times n_z$.

The formal solution of (1) with zero initial conditions is:

$$\mathbf{u}(t) = \int_0^t \frac{\sin \mathbf{L}(t-\tau)}{\mathbf{L}} \, \mathbf{f}(\tau) \, d\tau.$$

Here the source term needs to be separable in space and time, i.e.,

$$\mathbf{f}(\mathbf{x}, t) = \mathbf{g}(\mathbf{x}) \; h(t). \tag{3}$$

If we want to perform reverse-time modelling time-reversed seismogram sections need to be applied as sources. In this case the condition that the source is separable (equation 3) is not applicable since the individual seismograms all have different time histories. Therefore, we need to use the formal solution with non-vanishing initial conditions:

$$\mathbf{u}(t) = \cos \mathbf{L}t \; \mathbf{u}(0) + \frac{\sin \mathbf{L}t}{\mathbf{L}} \; \dot{\mathbf{u}}(0), \tag{4}$$

where the dot denotes the time derivative. We also need to have the formal solution at time $-t$, i.e.,

$$\mathbf{u}(-t) = \cos \mathbf{L}t \ \mathbf{u}(0) - \frac{\sin \mathbf{L}t}{\mathbf{L}} \ \dot{\mathbf{u}}(0) \tag{5}$$

to eliminate the term with $\dot{\mathbf{u}}(0)$. Here, we use the fact that the $\sin$ and $\cos$ functions are odd and even functions, respectively. Though $\mathbf{u}$ is a function of the position vector $\mathbf{x}$ and the time t for conciseness we dropped the spatial dependence. Adding equations 4 and 5 and solving for $\mathbf{u}(t)$ yields:

$$\mathbf{u}(t) = -\mathbf{u}(-t) + 2 \cos \mathbf{L}t \ \mathbf{u}(0). \tag{6}$$

This allows to extrapolate the field $\mathbf{u}(t)$ from the fields $\mathbf{u}(-t)$ and $\mathbf{u}(0)$ at two previous time instances in a similar manner as known from finite-difference time-stepping. It remains to transform the formal solution into a form which can be solved numerically. In an analogous way to the expansion of the $\sin$ function in the formal solution with zero initial conditions in Kosloff et al. (1989) we can expand the $\cos$ function:

$$\cos \mathbf{L}t = \sum_{k=0}^{\infty} c_{2k} \ J_{2k}(tR) \ Q_{2k} \left(\frac{i\mathbf{L}}{R} \right), \tag{7}$$

where $c_0 = 1$ and $c_k = 2$ if $k \neq 0$. J_n are the n-th order Bessel functions and Q_n are modified Chebyshev polynomials. R is related to the largest Eigenvalue of the operator $i\mathbf{L}$. To maintain convergence in the 2D case

$$R > \pi \, v_{max} \sqrt{(\Delta x)^{-2} + (\Delta z)^{-2}}, \tag{8}$$

where v_{max} is the highest velocity in the numerical grid. Δx and Δz are the grid spacings. The modified Chebyshev polynomials satisfy the recurrence

$$Q_{n+1}(x) = 2x \ Q_n(x) + Q_{n-1}(x) \tag{9}$$

with $Q_0(x) = 1$, $Q_1(x) = x$ and $Q_2(x) = 2x^2 + 1$. The modified Chebyshev polynomials are defined in terms of the usual Chebyshev polynomials: $Q_n(x) := i^n \ T_n(-ix)$, where T_n are the ordinary Chebyshev polynomials.
Since only even indexed terms appear in the expansion (equation 7) we use the following recurrence relation which can be derived from equation 9:

$$Q_{n+2}(x) = (4x^2 + 2) \ Q_n(x) - Q_{n-2}(x). \tag{10}$$

To initiate the recurrence we need the terms $Q_0(\frac{i\mathbf{L}}{R})\mathbf{u} = \mathbf{I}\mathbf{u}$ and $Q_2(\frac{i\mathbf{L}}{R})\mathbf{u} = -2\,\mathbf{L}^2\mathbf{u} + \mathbf{I}\mathbf{u}$, where we have replaced x by $\frac{i\mathbf{L}}{R}$. $\mathbf{I}$ is the identity matrix operator.
Of course, in the numerical evaluation of the expansion (7) only a finite number of terms will be used. For convergence the highest index should be slightly larger than tR, i.e., $M > tR$ (see Tal-Ezer et al. (1987)). The expansion for the REM approach where only even indexed terms occur then reads:

$$\cos \mathbf{L}t = \sum_{k=0}^{M/2} c_{2k} \ J_{2k}(tR) \ Q_{2k} \left(\frac{i\mathbf{L}}{R} \right). \tag{11}$$

The above discussion on the estimation of the number of expansion terms applies to the original REM method with source term (zero initial conditions) where usually at least several hundreds or a few thousands of terms are used to span several seconds of propagation time.
In case of time-stepping with small time increments Δt of, say, 1, 2 or 4 ms the maximum order of terms in the expansion is about 10–20 and the above criterion ($M > tR$) for the number of terms does not hold. To estimate a reasonable number of terms it is advisable to use as many terms until the ratio of the smallest to the largest coefficients, i.e. $J_{2k}(\Delta tR)$, is smaller than (single precision) relative machine accuracy which is about $10^{-6} - 10^{-7}$. Using less terms may be sufficient if the total propagation time is small. This accelerates the computations accordingly.

To perform a single time-step the following expression must be computed:

$$\mathbf{u}(t+\Delta t) = -\mathbf{u}(t-\Delta t) + 2 \sum_{k=0}^{M/2} c_{2k}\ J_{2k}(\Delta t R)\ Q_{2k}(\frac{i\mathbf{L}}{R})\,\mathbf{u}(t). \tag{12}$$

The $M/2+1$ Bessel functions J_{2k} are the same for any of the time-steps. Therefore, they can be computed beforehand. They only depend on the time-step size, the grid spacing, and the highest velocity of the modelling grid.

MODELLING EXAMPLES

To compare the usual 2nd order finite-difference time-stepping and the REM method 2D modelling examples were performed. In the following numerical examples the Fourier method was used for the calculations of spatial derivatives. For simplicity the acoustic wave equation is solved. The medium has constant velocity of 1500 m/s. It is discretized with 15 m in both, the x- and the z-direction. The source time history is Ricker-like with a maximum frequency of 50 Hz. The dominant frequency is about 25 Hz. The numerical grid consists of 1001×1001 grid nodes. The source is located at grid point index (100, 500) and the two receivers are at (110, 510) and (950, 510) which results in propagation distances of about 212 m and 12751 m, respectively. These distances are equivalent to approximately 3.5 and 212 dominant wavelengths, respectively. The numerical solutions are tested against the analytical solutions. The analytic solution is based on a Cagniard-deHoop technique (see e.g. Aki and Richards (1980)).

In Figures 1-3 comparisons with 2nd order finite-difference time integration are shown. The time-step sizes are 1 ms, 0.5 ms, and 0.25 ms, respectively. Given the above mentioned parameters the stability limit of the algorithm is about 4.5 ms. Even the largest of the above time-step sizes is well below this limit. Figure 1 shows that an unacceptable large amount of numerical dispersion occurs at large propagation distances if the time-step size is 1 ms. Reduction of the time-step size to 0.5 ms (Figure 2) improves the results a lot. Some discrepancies can still be observed compared to the analytic solution. Decreasing the time-step size further to 0.25 ms the seismograms of Figure (3) are almost indistinguishable.

The examples shown in Figures 4-6 were calculated using the REM approach with 4 ms time-step size and with different degrees of accuracy. The different degrees of accuracy result from different numbers of terms in the temporal Chebyshev expansion. The annotated accuracies in Figures 4-6 reflect the ratio of the smallest to the largest coefficient in the expansion. The Bessel functions are the coefficients in this context. As can be seen from Figure 4 there are some discrepancies in the seismograms even for small propagation distances, which become much larger for the large distances if the accuracy is set to 10^{-2}. Obviously, the number of expansion terms is not sufficient to obtain convergence. Increase of the accuracy (10^{-4}) results in a much better match for the comparison with the analytic solution (Figure 5). However, at large distances there is still a slight deviation. Using accuracy of 10^{-6} which is about single precision machine accuracy the match is very good even at large distance (Figure 6).

Comparison of computational times

In the modelling algorithms based on the Fourier method most of the CPU time is spent for the calculation of the operator $-\mathbf{L}^2$. This is due to the fact that the spatial derivatives are computed using Fourier transforms (FFTs). Therefore, the number of evaluations of $-\mathbf{L}^2$ is essentially a measure of the performance. In the above examples in total 10 seconds propagation time was simulated where different numbers of evaluations of the operator $-\mathbf{L}^2$ were required to achieve certain accuracies of the modelling results. For the 2nd order FD time integration one evaluation per time-step is needed. In case of the REM approach where the time-step size was fixed to 4 ms the number of operator evaluations depend on the desired accuracy. Note that the number of operator evaluations is always one less than the number of expansion terms, since the zero order term requires no $-\mathbf{L}^2$ evaluation. Table 1 lists the number of evaluations needed for the modelling runs. The right column shows the total number of evaluations for the different modelling runs. Graphical results of the runs based on the REM approach with 2 ms time-step size given in Table 1 are not

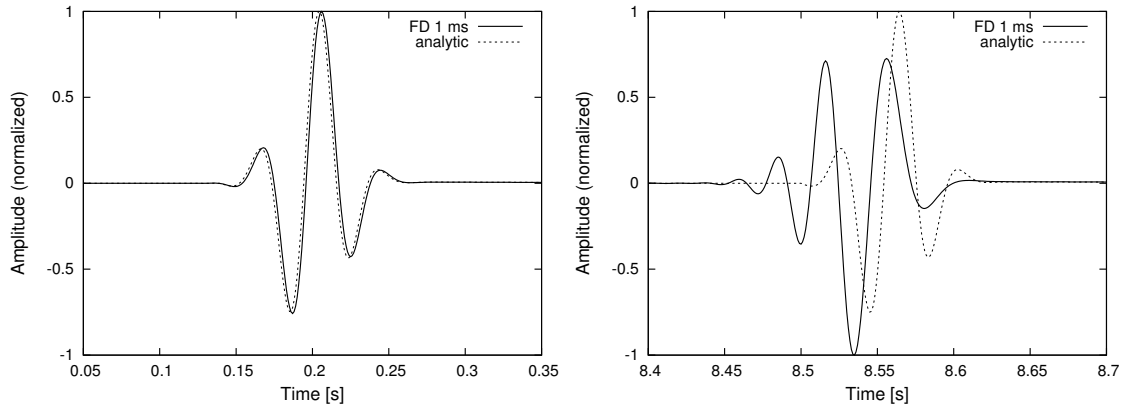

Figure 1: Comparison of FD time integration with $\Delta t = 1$ ms with analytic solution at 3.5 (left) and 212 (right) dominant wavelengths distance.

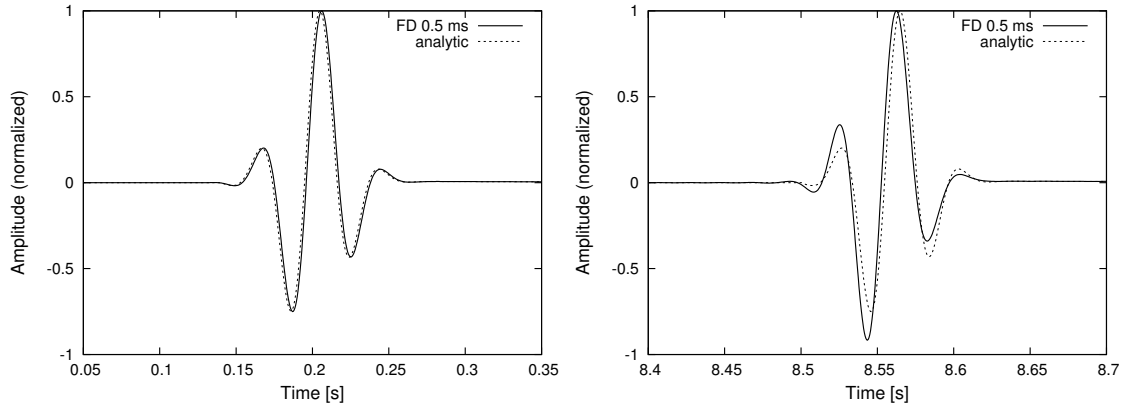

Figure 2: Comparison of FD time integration with $\Delta t = 0.5$ ms with analytic solution at 3.5 (left) and 212 (right) dominant wavelengths distance.

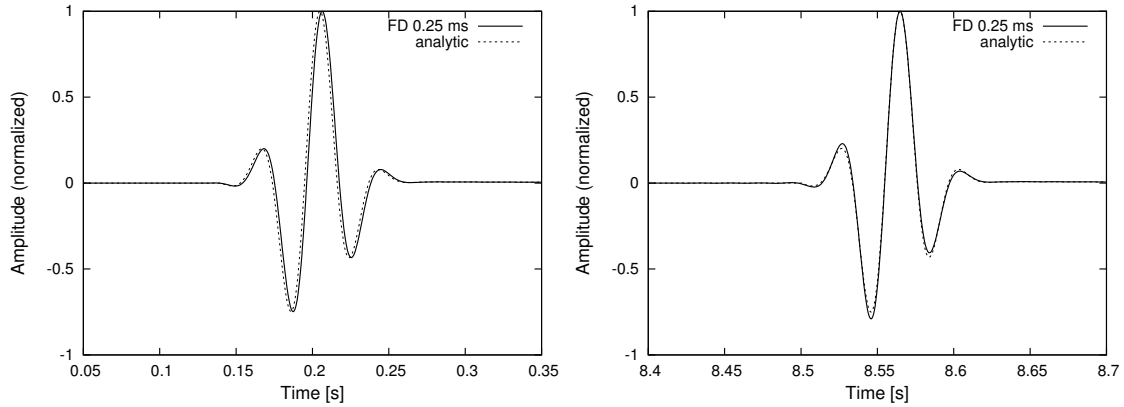

Figure 3: Comparison of FD time integration with $\Delta t = 0.25$ ms with analytic solution at 3.5 (left) and 212 (right) dominant wavelengths distance.

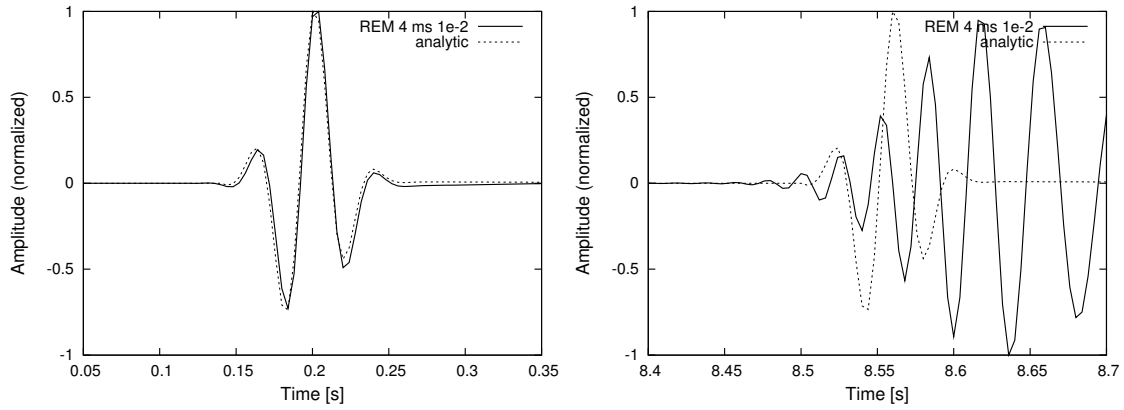

Figure 4: Comparison of REM time integration with relative accuracy down to 10^{-2} (4 expansion terms) with analytic solution at 3.5 (left) and 212 (right) dominant wavelengths distance.

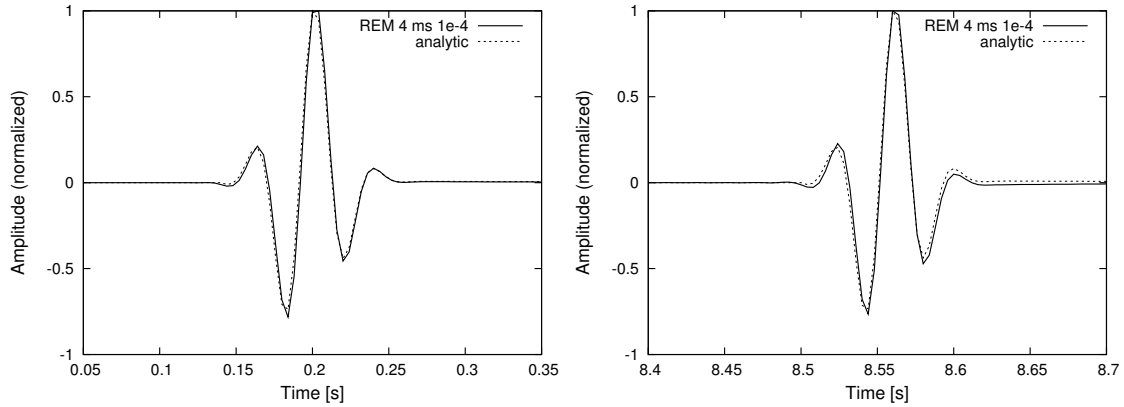

Figure 5: Comparison of REM time integration with relative accuracy down to 10^{-4} (5 expansion terms) with analytic solution at 3.5 (left) and 212 (right) dominant wavelengths distance.

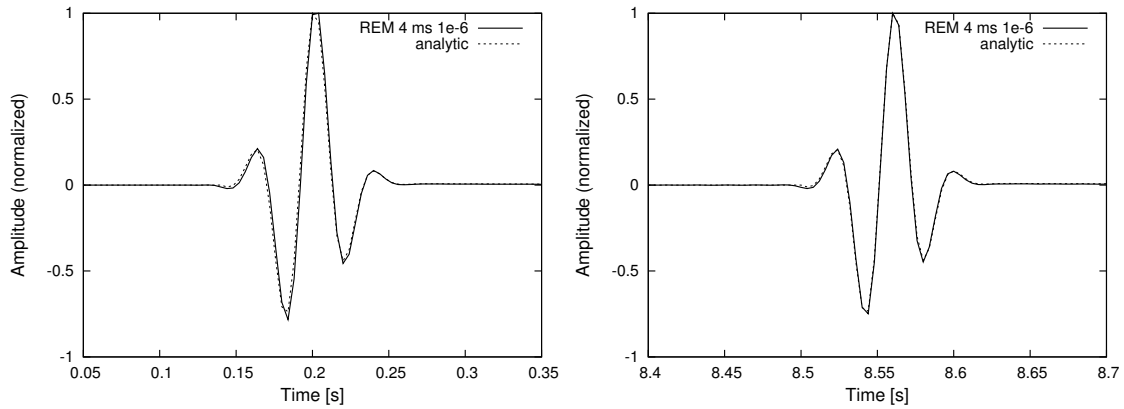

Figure 6: Comparison of REM time integration with relative accuracy down to 10^{-6} (6 expansion terms) with analytic solution at 3.5 (left) and 212 (right) dominant wavelengths distance.

shown here. They only differ in their smoother visual appearance compared to the seismograms sampled at 4 ms.

Algorithm	Steps	$-\mathbf{L}^2$/Step	Total
FD			
1 ms	10,000	1	10,000
0.5 ms	20,000	1	20,000
0.25 ms	40,000	1	40,000
REM (4 ms)			
10^{-2}	2,500	3	7,500
10^{-4}	2,500	4	10,000
10^{-6}	2,500	5	12,500
REM (2 ms)			
10^{-2}	5,000	2	10,000
10^{-4}	5,000	3	15,000
10^{-6}	5,000	4	20,000

Table 1: Number of evaluations of the operator $-\mathbf{L}^2$ for different algorithms with various time-step sizes and accuracies. Total propagation time in a homogeneous model is 10 seconds.

Modelling example with interface

To demonstrate the accuracy of the time-stepping REM approach in case of an inhomogeneous subsurface comparisons of numerical results with analytic solutions were done. Modelling parameters are the same as in the above homogeneous case except that the acoustic velocity is increased to 3000 m/s below 3500 m depth and that the source and receiver positions are different: the source is located at (1000 m, 3000 m) and the receivers are positioned at (1400 m, 3100 m) and (3000 m, 3100 m). The comparison of the seismograms in Figure 7 at 400 m (left) and 2000 m (right) horizontal offset from the source shows very good agreement. Both figures show the direct wave and the reflection from the interface. The small amplitude precursor in the right panel of the figure at about 1.8 s propagation time is the head wave arrival.

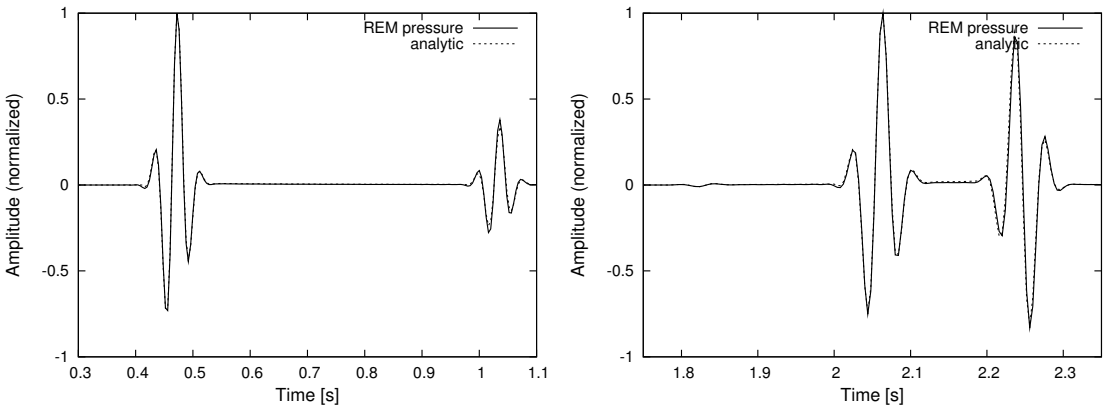

Figure 7: Comparison of REM seismograms with analytic solutions. Left: 400 m horizontal offset. Right: 2000 m offset. In both seismograms the direct wave and the reflection can be observed. The precursor at about 1.8 s propagation time in the right panel is the head wave arrival.

POYNTING VECTOR COMPUTATIONS WITH REM

For estimation of the propagation direction of energy the Poynting vector can be calculated. For the computation of the Poynting vectors time derivatives of the seismograms are required. These time derivatives can be computed by the REM approach together with the seismograms at almost no extra cost. Details are given in Appendix A.
In reverse-time migration, the Poynting vector allows to estimate the scattering angle between the wave fields of the forward modelled shot and the reversely modelled shotgather. This can be useful if there is low frequency noise in the migrated image due to very large scattering angles. A snapshot of the directions of energy propagation for a model with two homogeneous layers separated by a horizontal interface at 1300 m depth is shown in Figure 8. The model consists of 231×231 grid nodes with 10 m grid spacing. The

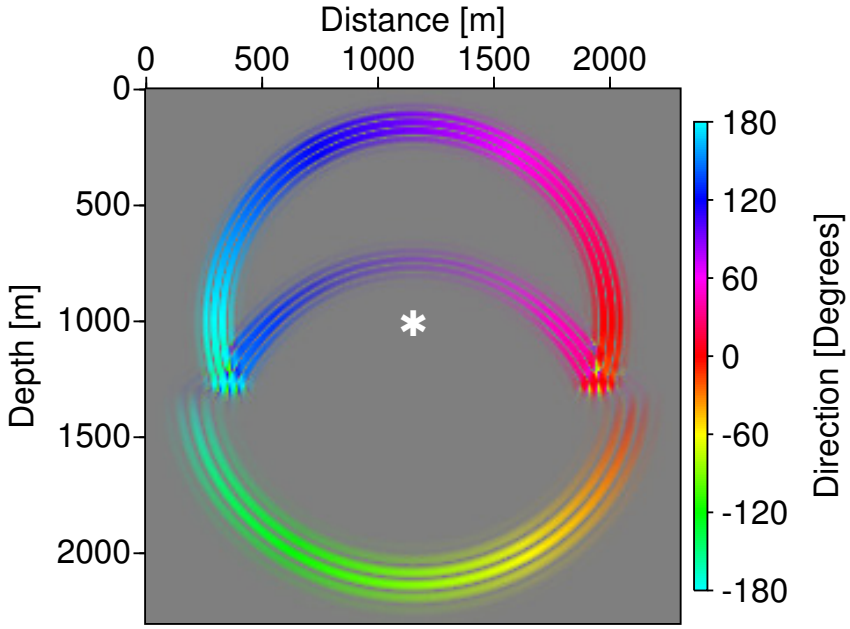

Figure 8: Poynting vector snapshot of a two-layer case. The colors indicate the direction of energy propagation. The color intensity is proportional to the energy amplitude. The source location is marked by an asterisk.

velocities in the first and second layer are 2000 m/s and 3000 m/s, respectively. The source with a 50 Hz cut-off frequency Ricker wavelet is at (1150 m, 1000 m). Time steps of 2 ms were chosen. The snapshot was taken at 480 ms.
To demonstrate that the numerical result of the time derivative of the seismograms computed by the REM approach is of similar accuracy as that of the seismograms a comparison with the analytic solution is presented in Figure 9. This trace is the time derivative of the trace shown in the right panel of Figure 6. The setup of the modelling is the same as in the homogeneous example. Also here the trace is at a distance of 212 dominant wavelengths. For the computation of the time derivative the operator of equation 21 was applied.

PRESTACK REVERSE-TIME MIGRATION USING REM

For the application of REM in prestack reverse-time migration a simple heterogeneous 2D subsurface model was used to produce synthetic seismograms and to subsequently migrate the shotgathers. 35 shots with distances of 20 m were generated and migrated. The subsurface model is shown in Figure 10. The velocities in the different layers from top to bottom were 2000 m/s, 2500 m/s, 3000 m/s, and 2000 m/s,

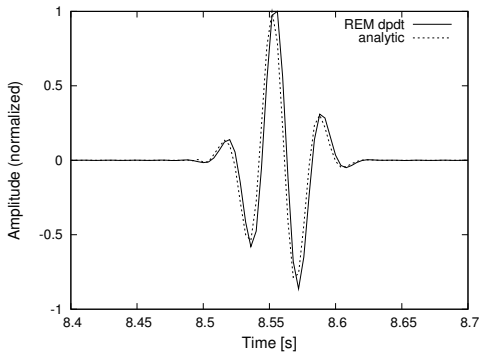

Figure 9: Comparison of the numerically computed time derivative of the seismogram and the analytic solution for the homogeneous case at a distance of 212 dominant wavelengths.

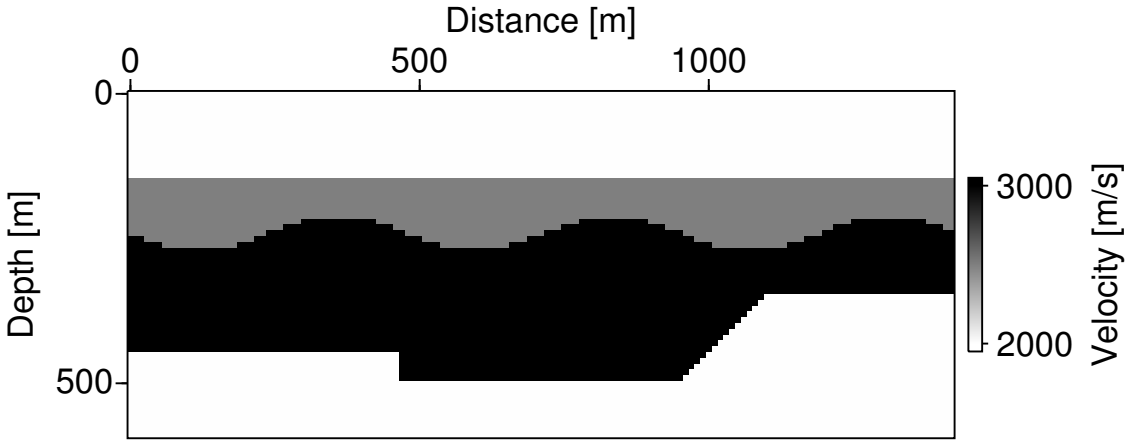

Figure 10: Subsurface velocity model used for forward modelling and reverse-time migration.

respectively. The numerical grid consists of 143×117 grid nodes in total. The source time signal is a 100 Hz Ricker wavelet. The time-step size is 2 ms with 800 ms total propagation time. The images were produced in a vertically 60 grid points wide stripe. Absorbing boundaries of 20 grid points width were applied at the borders of the numerical grid (Cerjan et al. (1985)). The chosen accuracy with respect to the expansion coefficients was 10^{-6}. The stack of 35 images without limitation of scattering angles is shown in Figure 11. Low frequency noise represented by black background colors is present in the stacked image. In Figure 12 the stack of 35 migrated images where the scattering angles were limited to 120 degrees is shown. The low frequency noise is greatly reduced.

CONCLUSIONS

It is known that the Rapid Expansion Method generates more accurate results than the usual 2nd order finite-difference time integration. Therefore, the application of the Rapid Expansion Method to seismic modelling problems is preferable. Moreover, REM needs less evaluations of the operator $-\mathbf{L}^2$ at higher accuracy and is therefore more efficient. For seismic problems like reverse-time migration the original implementation is not suitable since in such an algorithm the time-histories of the reinjected shot-gather traces are all different and the source term is not separable. Therefore, the algorithm needs to be implemented in a time-stepping manner where the time integration of each time-step is performed using the temporal Chebyshev expansion.

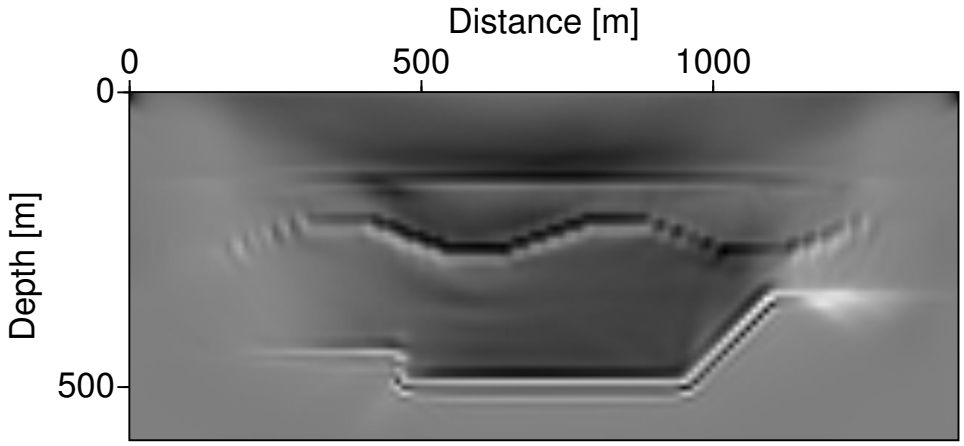

Figure 11: Stack of 35 images without limitation of scattering angles.

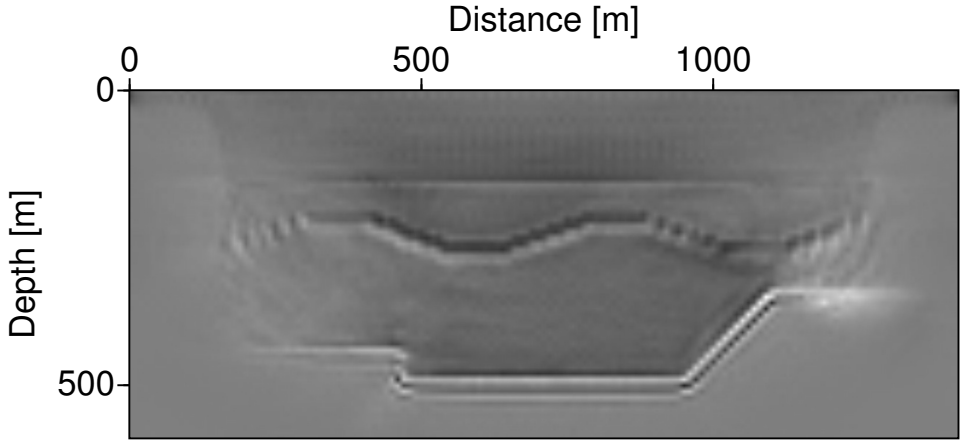

Figure 12: Stack of 35 images with scattering angles limited to 120 degrees.

When considering only small propagation times it appears that REM is more costly since the ratio of the number of expansion terms to the propagation time is higher for small time-steps than for large time-steps. However, if large propagation times are considered, which is normally the case in field data applications, it turns out that 2nd order finite-difference time integration requires a large number of very small time increments in order to reduce numerical dispersion. In such situations the REM approach with time-stepping is more efficient and at the same time more accurate. This was proven with numerical examples and comparisons with analytic solutions.
It is demonstrated how it is possible to integrate the calculations of Poynting vectors where the time derivative of the solution of the wave equation is required. This derivative is not delivered by the original REM algorithm but can be easily derived from available quantities at minimal extra cost.
Migration results for a simple synthetic example confirm the ability of the REM approach to handle Poynting vector calculations successfully.

ACKNOWLEDGMENTS

This work was kindly supported by the University of Hamburg and the sponsors of the WIT consortium. I thank Dan Kosloff for the analytic solution program.

REFERENCES

Abramowitz, M. and Stegun, I. (1972). *Handbook of mathematical functions*. Dover Publications.

Aki, K. and Richards, P. (1980). *Quantitative Seismology: Theory and Methods*. W.H. Freeman & Co.

Cerjan, C., Kosloff, D., Kosloff, R., and Reshef, M. (1985). A non-reflecting boundary condition for discrete acoustic and elastic wave calculation. *Geophysics*, 50:705–708.

Crase, E. (1990). High-order (space and time) finite-difference modeling of the elastic wave equation. In *Exp. Abstr.* Soc. Explor. Geophys. (SEG).

Dablain, M. (1986). The application of high-order differencing to the scalar wave equation. *Geophysics*, 51:54–66.

Kosloff, D., Fihlo, A., Tessmer, E., and Behle, A. (1989). Numerical solution of the acoustic and elastic wave equations by a new rapid expansion method. *Geophysical Prospecting*, 37:383–394.

Pestana, R. and Stoffa, P. (2009). Rapid expansion method (REM) for time-stepping in reverse time migration (RTM). In *Exp. Abstr.* Soc. Explor. Geophys. (SEG).

Tal-Ezer, H., Kosloff, D., and Koren, Z. (1987). An accurate scheme for seismic forward modeling. *Geophys. Prosp.*, 35:479–490.

Yoon, K., Marfurt, K., and Starr, W. (2004). Challenges in reverse-time migration. In *Exp. Abstr.* Soc. Explor. Geophys. (SEG).

APPENDIX A

Poynting vector

To use Poynting vector information, e.g., the directions of energy transport, for improving the image quality (Yoon et al. (2004)) not only the solution of the wave equation $\mathbf{u}(t)$ is required. In addition its first time derivative $\dot{\mathbf{u}}(t)$ needs to be at hand. This is not automatically provided when using the REM method.
In the case of the acoustic wave equation the Poynting vector $\mathbf{S}$ is proportional to

$$\mathbf{S} \propto -\nabla p \frac{dp}{dt} p. \tag{13}$$

Calculation of the time derivative of the solution

The time derivative of the pressure field can be obtained in a relatively simple way at almost no extra cost in terms of CPU time.
Starting from the formal solution with non-vanishing initial conditions (equation 6):

$$\mathbf{u}(t) = -\mathbf{u}(-t) + 2\,\cos \mathbf{L}t\;\mathbf{u}(0) \tag{14}$$

the time derivative is $[\cos \mathbf{L}t]' = -\mathbf{L} \sin \mathbf{L}t$:

$$\dot{\mathbf{u}}(t) = \dot{\mathbf{u}}(-t) - 2\;\mathbf{L} \sin \mathbf{L}t\;\mathbf{u}(0). \tag{15}$$

Therefore, we need an expansion of the operator $-\mathbf{L} \sin \mathbf{L}t$ with respect to modified Chebyshev polynomials:

$$i\;\sin \mathbf{L}t = \sum_{k=0}^{\infty} c_{2k+1}\;J_{2k+1}(tR)\;Q_{2k+1}\left(\frac{i\mathbf{L}}{R}\right) \tag{16}$$

$$\Rightarrow -\mathbf{L}\ \sin \mathbf{L}t = \sum_{k=0}^{\infty} c_{2k+1}\ J_{2k+1}(tR)\ i\mathbf{L}\ Q_{2k+1}\left(\frac{i\mathbf{L}}{R}\right) \tag{17}$$

or

$$-\mathbf{L}\ \sin \mathbf{L}t = \sum_{k=0}^{\infty} c_{2k+1}\ R\ J_{2k+1}(tR)\ \frac{i\mathbf{L}}{R}\ Q_{2k+1}\left(\frac{i\mathbf{L}}{R}\right) \tag{18}$$

Therefore, we essentially need to calculate terms of the form $x\ Q_{2k+1}(x)$.
From the recurrence equation 9:

$$Q_{n+1}(x) = 2x\ Q_n(x) + Q_{n-1}(x) \tag{19}$$

we find if we rearrange terms and shift the indices:

$$x\ Q_{n-1}(x) = \frac{Q_n(x) - Q_{n-2}(x)}{2}. \tag{20}$$

In our operator notation this reads:

$$\frac{i\mathbf{L}}{R}\ Q_{2k-1}\left(\frac{i\mathbf{L}}{R}\right) = \frac{Q_{2k}\left(\frac{i\mathbf{L}}{R}\right) - Q_{2k-2}(\frac{i\mathbf{L}}{R})}{2}. \tag{21}$$

The terms $Q_{2k}\left(\frac{i\mathbf{L}}{R}\right)\mathbf{u}$ and $Q_{2k-2}\left(\frac{i\mathbf{L}}{R}\right)\mathbf{u}$ have already been computed during the expansion of the $\cos \mathbf{L}t$ operator in equation 7. Here, however, the odd indexed Bessel functions are used.

An alternative way to yield the time derivative of the solution is to use a different set of coefficients for weighting the even indexed modified Chebyshev polynomials: here, instead of the $J_{2k}(tR)$ we take the derivatives $J'_{2k}(tR)$ as the coefficients.
The derivative of the Bessel functions J'_n can be calculated using the relations

$$J'_n(x) = J_{n-1} - \frac{n}{x}\ J_n(x)$$

or

$$J'_n(x) = -J_{n+1} + \frac{n}{x}\ J_n(x)$$

(see e.g. Abramowitz and Stegun (1972), p.361, 9.1.27).

Numerical estimation of Bessel functions

Bessel functions satisfy the recurrence relation:

$$J_{n-1}(x) + J_{n+1}(x) = \frac{2\,n}{x}\ J_n(x) \tag{22}$$

For a given argument x the Bessel functions $J_n(x)$ can be computed by a downward recurrence if $n > x$. According to Abramowitz and Stegun (1972) we can arbitrarily set $J_{n+1}(x) = 0$ and $J_n(x) = 1$. Using equation 22 all $J_n(x)$ can be calculated by decreasing the index successively until $J_0(x)$ is reached. The result needs to be normalized. The following property of the Bessel functions (Abramowitz and Stegun (1972), 9.1.46) allows to find the normalization factor:

$$J_0 + 2\,J_2 + 2\,J_4 + \cdots = 1.$$

Note that the Bessel function values of the highest orders computed in this way are not very accurate. Therefore, one should start the recurrence at higher orders than actually needed. If the maximum required order is M then it is safe to start the recurrence at $M + 50$. Since the Bessel functions need to be computed in the beginning of the modelling for only one single argument, i.e. $J_n(\Delta t\,R)$, this extra amount of computational work can be neglected. For the computations of the Bessel functions double precision arithmetic should be used.